

The Shift in Bandgap and Dielectric Constant Due to lattice Expansion in $\text{CH}_3\text{NH}_3\text{SnI}_3$ Using FHI-aims

^{*1}Hassan Abdulsalam and ²Garba Babaji

¹Department of Physics, Yobe State University, Damaturu P.M.B.1144, Yobe Nigeria.

²Department of Physics, Bayero University, Kano P.M.B. 3011, Kano Nigeria

*Corresponding Author Email: habdulsalam@ysu.edu.ng

(Received 21 June 2018, Accepted 19 August 2018, Published 13 September 2018)

Abstract: Although methyl ammonium lead iodide, ($\text{CH}_3\text{NH}_3\text{PbI}_3$) has proven to be an effective photovoltaic material, there remains a main concern about the toxicity of lead, therefore determination of a lead free halide perovskite is of outstanding interest. Sn^{2+} metal cations are the most obvious substitute for Pb^{2+} in the perovskite structure because of the similar s^2 valence electronic configuration to Pb^{2+} . Sn^{2+} can form a perovskite with a basic formula ASnX_3 ($\text{A} = \text{CH}_3\text{NH}_3$ and $\text{X} = \text{halide}$) because the ionic radius of Sn^{2+} is similar to that of Pb^{2+} . With the above similarity, methyl ammonium tin iodide $\text{CH}_3\text{NH}_3\text{SnI}_3$ is one of the common replacement for $\text{CH}_3\text{NH}_3\text{PbI}_3$ in the fabrication of organic-inorganic perovskite solar cells. FHI-aims code was used to perform the simulation of $\text{CH}_3\text{NH}_3\text{SnI}_3$ in this work. Geometry building, parameter optimization, determination of the best exchange functional, k-grid convergence test along with determination of equilibrium lattice constant and geometry relaxation for $\text{CH}_3\text{NH}_3\text{SnI}_3$ were carried out. An energy direct band gap of 1.051 eV was obtained, with an underestimation of 0.249 eV which amount to 19.2% when compared with experimental value. The lattice constant obtained using phonopy with ZPE is close to experimental reported values with an underestimation of 3.01%. The temperature dependent of lattice constant was studied in the temperature range of 0 to 318 K. At the same temperature range, shift in energy bandgap and dielectric constant due to lattice expansion was also investigated.

Keywords: Methyl ammonium tin iodide ($\text{CH}_3\text{NH}_3\text{SnI}_3$), DFT, FHI-aims, Bandgap, Dielectric constant, linear-thermal-expansion

1. Introduction

The solid-state dye sensitized solar cells possess a monolithic structure in contrast to the sandwich design of the liquid electrolyte based DSSC. Processes such as photo excitation of sensitizer, electron injection and dye regeneration are the same as in the liquid electrolyte-based DSC, the only different part is that the transfer holes takes place directly from the dye to the hole transporting

material (HTM), and then the hole is transported via hopping to the counter electrode. Typically, the light-harvesting active layer is a hybrid organic-inorganic lead or tin halide-base material, the popular among is being methyl ammonium lead iodide, $\text{CH}_3\text{NH}_3\text{PbI}_3$ [1]. Perovskite materials such as the methyl ammonium lead halides are cheap to produce and simple to manufacture. Solar cell efficiencies of devices using these materials have increased from 3.8% in 2009[2] to a certified 20.1% in 2014, making this the fastest-advancing solar technology[1]. According to detailed balance analysis, the efficiency limit of perovskite solar cells is about 31%, which approaches the Shockley-Queisser of gallium arsenide which is 33% [3]. Their high efficiencies and low production costs make perovskite solar cells a commercially attractive option. At about 330 K $\text{CH}_3\text{NH}_3\text{PbI}_3$ exist in cubic crystal system, as the temperature decreases to about 236 K, the cubic phase is transformed into the tetragonal phase. As the temperature decreases lower to about 177 K, the tetragonal phase is transformed into orthorhombic crystal systems[4]. From above it is evident that temperature affect the crystal structures of $\text{CH}_3\text{NH}_3\text{PbI}_3$, and in turn the crystal structures of the perovskite-type compounds, strongly affect the electronic structures such as energy band gaps. Although methyl ammonium lead iodide, ($\text{CH}_3\text{NH}_3\text{PbI}_3$) has proven to be an effective photovoltaic material, there remains a main concern about the toxicity of lead. Lead-based perovskites are a major issue that may prejudice implementation of any PSC technology, both regulation and common sense suggest that PSCs have to become lead free to deliver a sustainable technology[5]. The determination of a lead free halide perovskite is of outstanding interest. Sn^{2+} metal cations are the most obvious substitute for Pb^{2+} in the perovskite structure because of the similar s^2 valence electronic configuration to Pb^{2+} . Sn^{2+} can form a perovskite with a basic formula ASnX_3 (A= CH_3NH_3 and X = halide) because the ionic radius of Sn^{2+} is similar to that of Pb^{2+} [6]. With the above similarity, methyl ammonium tin iodide $\text{CH}_3\text{NH}_3\text{SnI}_3$ is one of the common replacement for $\text{CH}_3\text{NH}_3\text{PbI}_3$ in the fabrication of organic-inorganic perovskite solar cells. In this work, effect of temperature on bandgap and dielectric constant of $\text{CH}_3\text{NH}_3\text{SnI}_3$ was studied using FHI-aims code.

2. Theoretical Background

2.1 Density Functional Theory

Density Functional Theory (DFT) is a quantum mechanical technique used in Physics and chemistry to investigate the structural and electronic properties of many body systems. DFT has proved to be highly successful in describing structural and electronic properties in a vast class of materials, ranging from atoms and molecules to simple crystals and complex extended systems (including gasses and liquids). Furthermore DFT is computationally very simple. For these reasons DFT has become a common tool in first-principles calculations aimed at describing or even predicting properties of molecular and condensed matter systems[7].

Traditional methods in electronic structure theory, in particular Hartree-Fock theory and its descendants are based on the complicated many-electron wave function. The main objective of density functional theory is to replace the many-body electronic wave function with the electronic

density as the basis quantity. Whereas the many-body wave function is dependent on $3N$ variables, three special variables for each of the N electrons, the density is only a function of three variables and is a simpler quantity to deal with both conceptually and practically. Consider a system of N interacting (spinless) electrons under an external potential $V(r)$ (usually the Coulomb potential of the nuclei). If the system has a non-degenerate ground state, it is obvious that there is only one ground-state charge density $n(r)$ that corresponds to a given $V(r)$. In 1964 Hohenberg and Kohn demonstrated the opposite, far less obvious result: there is only one external potential $V(r)$ that yields a given ground-state charge density $n(r)$. The demonstration is very simple and uses a *reduction ad absurdum* argument[8].

For many-electron Hamiltonian with ground state Wave function ψ is given by:

$$H = T + U + V \quad (1)$$

Where T is the kinetic energy, U is the electron-electron interaction, V is the external potential. The charge density $n(r)$ as defined by Hohenberg and Kohn in 1964 is

$$n(r) = N \int |\psi(r_1, r_2, r_3, \dots, r_N)|^2 dr_2 \dots dr_N \quad (2)$$

Considering a different Hamiltonian: $H' = T' + U' + V'$; with ground state wave function Ψ' . Assuming the ground state charge densities are the same; i.e. $n[V] = n'[V']$. Then the following inequality holds:

$$E = \langle \psi' H' \psi' \rangle < \langle \psi H' \psi \rangle = \langle \psi H + V' - V \psi \rangle \quad (3)$$

$$\text{That is: } E' < E + \int (V(r) - V'(r)) n(r) dr \quad (4)$$

The inequality is strict because ψ and ψ' are different, being eigenstate of different Hamiltonians. By reversing the primed and unprimed quantities, one obtains an absurd result. This demonstrates that no two different potentials can have the same charge density.

The major problem with DFT is the exact functional for exchange and correlation are not known except for the free electron gas. However approximations exist which permits the calculation of certain physical quantities quite accurately. In DFT the most widely used approximation is the local density approximation (LDA), where the functional depends only on the density at coordinate where the functional is evaluated:

$$E_{XC}^{LDA}[n] = \int n(\vec{r}) \epsilon_{XC}[n](\vec{r}) d\vec{r} \quad (5)$$

where $\epsilon_{XC}[n]$ is the exchange-correlation energy density of uniform electron gas. In principle the LDA should only work when the density of the electron gas is almost homogeneous. It has been, however, found to give very good results even when the density of electron gas varies rapidly[9].

The generalized gradient approximations (GGA) are still local but also take into account the gradient of the density at the same coordinate, it has the general form:

$$E_{XC}^{GGA}[n] = \int f(n(\vec{r}), \nabla n(\vec{r})) d^3\vec{r} \quad (6)$$

The following are some of the different parameterizations of generalized gradient approximations are; am05 (GGA functional designed to include surface effects in self-consistent density functional theory, according to Armiento and Mattsson), blyp (The BLYP functional: Becke exchange and

Lee-Yang-Parr correlation), pbe (GGA of Perdew, Burke and Ernzerhof) and pbeint (PBEint functional according to Fabiano, L. A Constantin and F. Della Sala) [9]. Many different kinds of functional have been developed, and there is no easy way to tell which the best is. Some work well in some situations and fail in others. Some rely on fitted parameters to experimental data while others have been derived purely from the theoretical basis.

2.2 Electronic Band Structure and Bandgap

The periodic crystal structure is one of the most important aspects of materials science as many properties of materials depend on their crystal structures. One of its most immediate consequences is the arrangement of the electronic states within bands. For semiconductors, many properties are determined from these bands[10]. The electronic band structure of a solid describes those ranges of energy that an electron within the solid may have and ranges of energy that it may not have[11]. Band theory derives these bands and band gaps by examining the allowed quantum mechanical wave functions for an electron in a large, periodic lattice of atoms or molecules. Band theory has been successfully used to explain many physical properties of solids, such as electrical resistivity and optical absorption and forms the foundation of the understanding of all solid-state devices. Band structure calculations take advantage of the periodic nature of a crystal lattice, exploiting its symmetry.

The electronic band gaps of Perovskite materials are determined by the states at the valence band maximum (VBM) and conduction band minimum (CBM). A requisite for PSC to work properly just like in DSSC, the LUMO level of the light harvester should be higher than the conduction band edge (CBE) of anode material[12]; for example in TiO_2 which is located at -4.0 eV [13]. This would provide the required driving force for a faster excited state electron injection. The magnitude of the band gap determines the onset of optical absorption and is closely related to the maximum voltage achievable in a photovoltaic device[14]. The energy band gaps of organic-inorganic perovskite increase with increasing lattice parameter, contrary to most general semiconductors like Si and GaAs, this is due to the electronic structure of the Perovskite materials[15]. It was found experimentally that the band gap of $\text{CH}_3\text{NH}_3\text{PbI}_3$ increases with lattice parameter, as evidenced by Photoluminescence (PL) results[16].

2.3 Dielectric Constant

The dielectric constant is obtained from the response of the material to an external electric field, it depends of the frequency of the applied electric field and is described by a tensor for anisotropic system. The dielectric tensor ϵ_r consists of a real part which represents the storage and an imaginary part which represents the loss[17]. The dielectric constant also called relative permittivity is value of the real part of the dielectric tensor at frequency equals to zero[18] i.e. $\text{Re}[\epsilon_r(\omega = 0)]$. The amount electric field attenuated in a substance compared to from a vacuum is indicated by its dielectric constant. Dielectric constant determines the magnitude of the coulomb interaction

between electron-hole pairs and charge carriers as well as any fixed ionic charges in the lattice, high dielectric constants are required for high efficiency solar cell. Dielectric constant for $\text{CH}_3\text{NH}_3\text{PbI}_3$ is in the range of 5–7[19].

2.4 Phonons: Harmonic Vibrations

In reciprocal space, the equation of motion for the vibration of a periodic array of harmonic atoms for each reciprocal vector \mathbf{q} is determined by dynamical matrix, $D(\mathbf{q})$.

$$D(\mathbf{q})v(\mathbf{q}) = \omega^2(\mathbf{q}) v(\mathbf{q}) \quad (7)$$

where $\omega^2(\mathbf{q})$ is eigenvalue, and $v(\mathbf{q})$ is eigenvector of the dynamical matrix $D(\mathbf{q})$ and they completely describe the dynamics of the system in the harmonic approximation, which is a superposition of harmonic oscillators, one for each eigenvalue[20].

The density of state, $g(\omega)$ is an important quantity;

$$g(\omega) = \sum_s \int \frac{d\mathbf{q}}{(2\pi)^3} \frac{1}{|\nabla\omega(\mathbf{q})|} \quad (8)$$

It allows the determination of any integrals (e.g. Helmholtz free energy) that only depends on eigenvalue, ω . The Helmholtz (vibrational) free energy $F^{ha}(T, V)$ which has no explicit dependence on the volume V is given by:

$$F^{ha}(T, V) = \int d\omega g(\omega) \left(\frac{\hbar\omega}{2} + k_B T \ln \left(1 - e^{-\left(\frac{\hbar\omega}{k_B T}\right)} \right) \right) \quad (9)$$

The heat capacity, C_V at constant volume can be determined from Helmholtz free energy[21];

$$C_V = -T \left(\frac{\partial F^{ha}(T, V)}{\partial T^2} \right)_V \quad (10)$$

2.5 Lattice Expansion in the Quasi-Harmonic Approximation

In an ideal harmonic system, which is fully determined by the dynamical matrix $D(\mathbf{q})$, its Hamiltonian does not depend on the volume, this implies that the harmonic Hamiltonian is independent of the lattice parameters, and as a consequence of this, the lattice expansion coefficient $\alpha(T)$ vanishes [20].

$$\alpha(T) = \frac{1}{a} \left(\frac{\partial a}{\partial T} \right)_P \quad (11)$$

To determine the temperature dependence of energy bandgap there is need to determine the lattice expansion. The quasi-harmonic approximation is used to account for the anharmonic effects in the determination of the lattice expansion[22]. The usage of the quasi-harmonic approximation requires the determination of how the phonons, i.e., the vibrational band structures and the associated free energies, change with the volume[21].

3. Methodology

In this work ab-initio calculation in the framework of density functional theory DFT, as implemented in the FHI-aims package was performed[23]. The generalized gradient approximation GGA with the blyp parameterization was employed for the evaluation of the exchange-correlation energy. Optimization of the followings configuration parameters; *occupation type (Gaussian or Fermi)*, *charge mix param*, *initial moment*, and *n max pulay* was also performed. The Gamma-centered grid method has been chosen for sampling the Brillion zone. Full relaxation of the atomic positions within the unit cell was performed following the Broyden-Fletcher Goldfarb-Shanno (BFGS) optimization algorithm. Optimal lattice constant was also determined for each structure. The **k**-paths ($\Gamma - X - M - \Gamma - R - X|M - R$) [24]was used in the band structure analysis. Energy band gap were calculated for the optimized geometries using the optimized configuration parameters.

To determine of how the vibrational band structures and the associated free energies, change with the volume of materials. The optimal lattice constant of the materials were determined by finding the minimum of the total energy $E_{DFT}(V)$ and $F^{ha}(T, V)$ by using the Birch-Murnaghan's equation of state[25]. Though, in the canonical ensemble, the relevant thermodynamic potential that needs to be minimized is the free energy $F(T, V)$ which is given by:

$$F(T, V) = E_{DFT}(V) + F^{ha}(T, V) \quad (12)$$

To account for the volume dependence of $F(T, V)$, the total energy, $E_{DFT}(V)$ and free energy, $F^{ha}(T, V)$ were calculated for a series of lattice constants. Eq. (12) was then evaluated and minimized using the Birch-Murnaghan's Equation of states, the phonopy program package and its FHI-aims interface phonopy-FHI-aims are used here. A FHI-aims python script titled *Compute_ZPE_and_lattice_expansion.py* [21] is used to perform the above procedure, this script requires the following inputs; optimal (equilibrium) lattice constant, the temperature range (0 to 318 K) and geometry information. The script gives two output files; one contains temperature, the lattice constant and the lattice expansion coefficient and the other contains the equilibrium lattice constant computed with and without zero point energy (ZPE). The investigation of the temperature dependence of the electronic band gaps of materials was carried out using a second python script titled *Compute_bandgap_at_different_volumes.py* [21]. Here electronic band structure calculations were performed for geometries constructed using the lattice constants generated from by the first script for temperature range of 0 to 308 K in a step of 11 K. This script gives an output file that contains both the lattice constants and the energy bandgap as a function of temperature. To obtain the linear dielectric tensor in FHI-aims the tag *compute_dielectric* is added in control.in file. It calculates and output the component of the imaginary and real part of the inter-band and intra-band contribution to the linear dielectric tensor. The linear dielectric tensor was determined in [100], [010] and [001] cubic directions for temperature range of 0 to 308 K in a step of 22 K.

4. Results and Discussion

The LUMO, HOMO, energy bandgap and lattice constant calculated are given in Table 1 along with reported theoretical and experimental band gap values where available.

Table 2. The comparison of Energy Bandgap and Lattice constant for $\text{CH}_3\text{NH}_3\text{SnI}_3$

		This work	Reported	
			Theoretical	Experimental
LUMO (eV)		-4.07492815	-	-
HOMO (eV)		-5.12601223	-	-
Bandgap (eV)		1.051	0.169[15]	1.30[26]
Lattice constant	From Single point calculation	6.033	6.163	6.24[27]
	From phonopy without ZPE	6.026		
	From phonopy with ZPE	6.049		

The bandgap evaluated in this work for $\text{CH}_3\text{NH}_3\text{SnI}_3$ has an underestimation of 0.249 eV which amount to 19.2% with experimental reported value.

In **Fig.1 (a)** linear thermal expansion coefficient, α given in Eq. (11) was plotted against temperature for temperature range of 0 to 318 K, while in **Fig. 1 (b)** shows the same plot but for temperature range of 0 to 25 K for more clarity. In **Fig. 2** shows the graph of lattice constant against temperature, **Fig. 3.** Shows the shift in bandgap due to lattice expansion. The lattice constant obtained using phonopy with ZPE is close to experimental reported values with an underestimation of 3.01%. Figure 1(a) shows that the linear thermal expansion coefficient does not change constantly with temperature, and it is negative for some very low temperatures, but in Figure 1(b) the negative expansion (contraction) can be seen to occur between the temperature ranges of 0 to 3K. There is a constant increment of the expansion coefficient at temperatures above 3K. The negative expansion observed for this materials is similar to those observed in some semiconductors such as Germanium, Silicon, Diamond and Gallium Arsenide[26]. The changes in lattice constant and bandgap with temperature is the same; little changes were observed at lower temperatures (0 to 3 K) for both lattice constant and bandgap [**Figs. 2 and 3**], it is obvious the bandgap varies linearly with lattice constant as shown in **Fig. 4**, the band gap increase with increasing lattice parameter like in most perovskite materials[15], contrary to most general semiconductors like Si and GaAs.

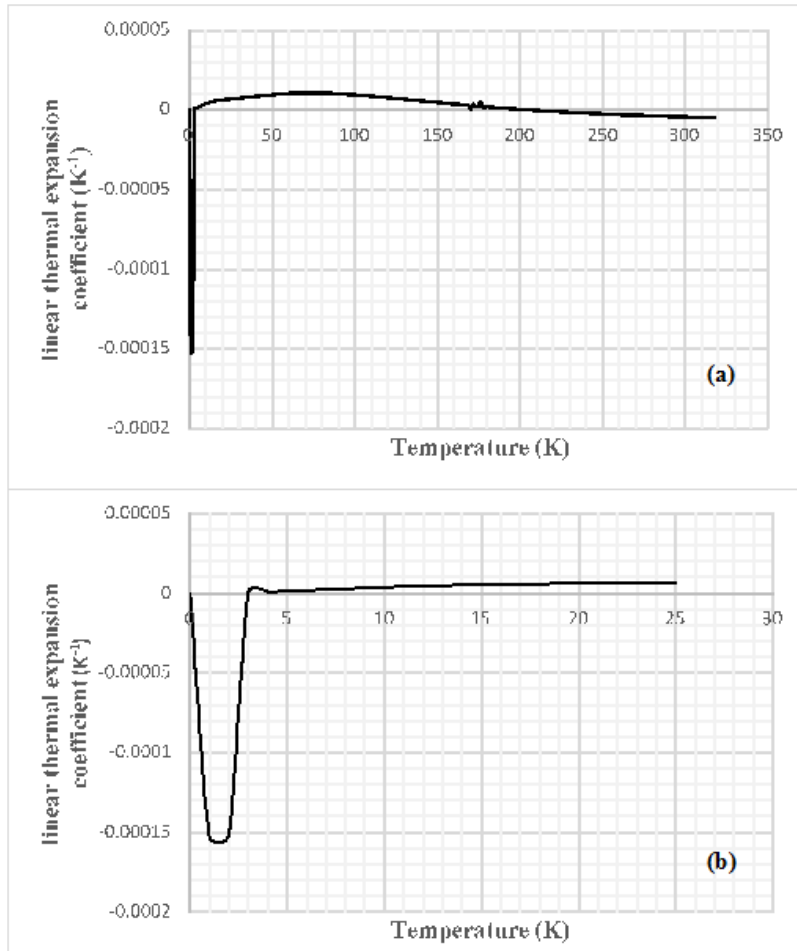


Fig. 1 Graph of linear thermal expansion coefficient against temperature
 (a) for range of 0 to 318 K and (b) for range of 0 to 25 K

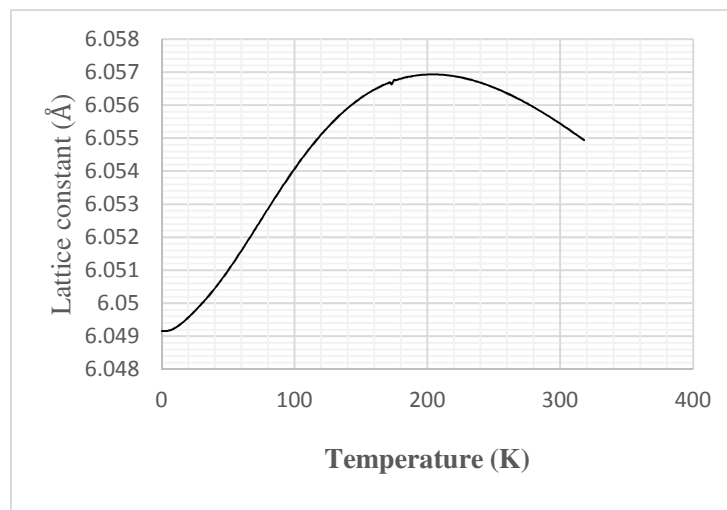


Fig. 2 Graph of lattice constant against temperature: for temperature range of 0 to 308 K
 in a step of 11 K

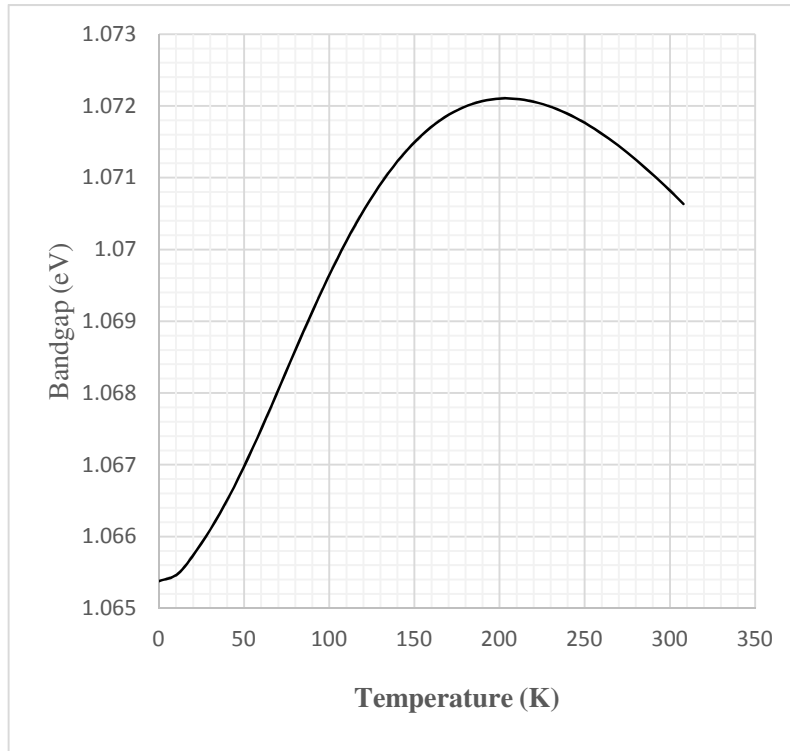


Fig. 3 Graph of bandgap against temperature: for temperature range of 0 to 308 K in a step of 22 K

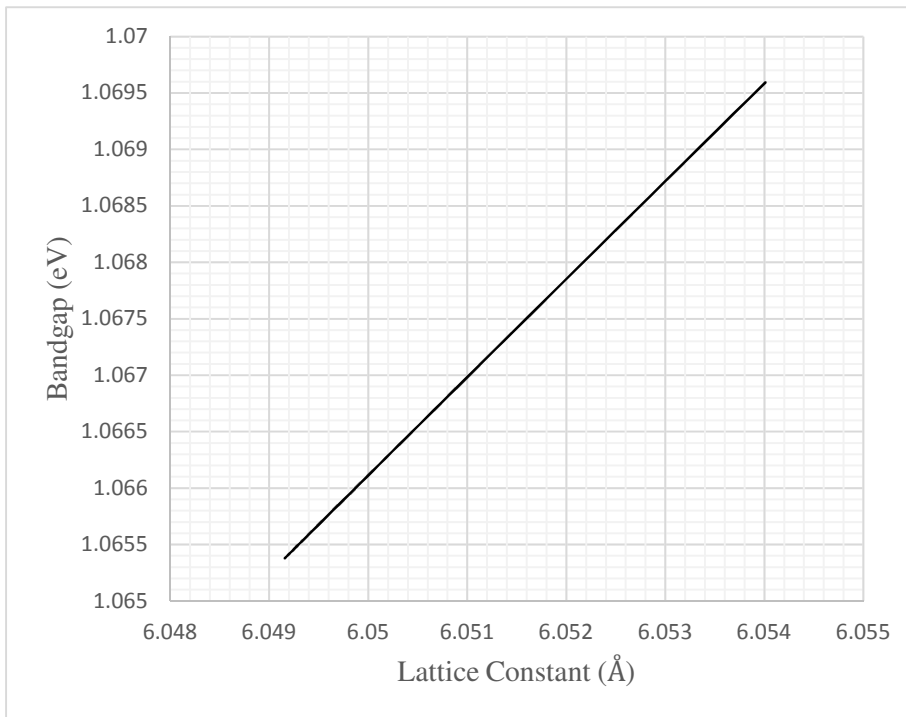


Fig. 4 . Graph of bandgap against lattice constant

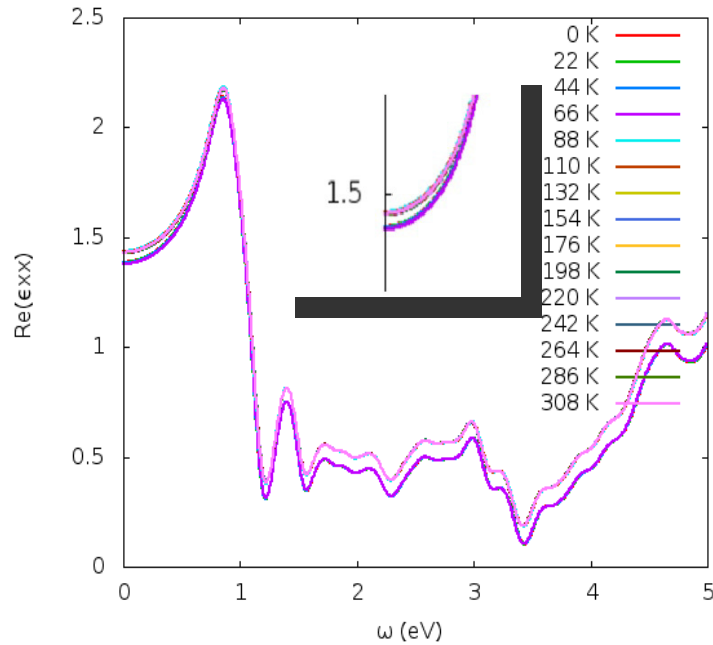


Fig. 5 Graph of Real components of complex dielectric tensor against frequency in [100] direction for temperature range of 0 to 308 K in a step of 22 K., insert shows dielectric tensors at frequency equals to zero (i.e. $Re [\epsilon_{xx} (\omega = 0)]$)

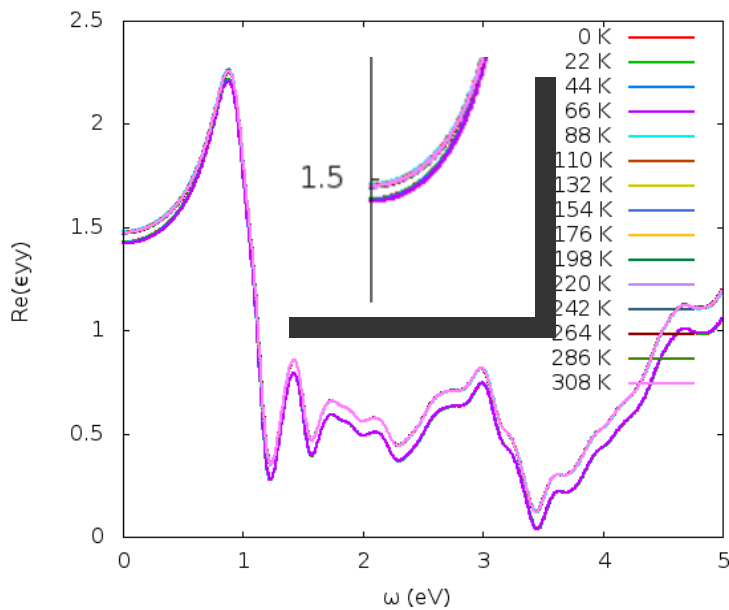


Fig. 6 Graph of Real components of complex dielectric tensor against frequency in [010] direction for temperature range of 0 to 308 K in a step of 22 K., insert shows dielectric tensors at frequency equals to zero (i.e. $Re [\epsilon_{yy} (\omega = 0)]$)

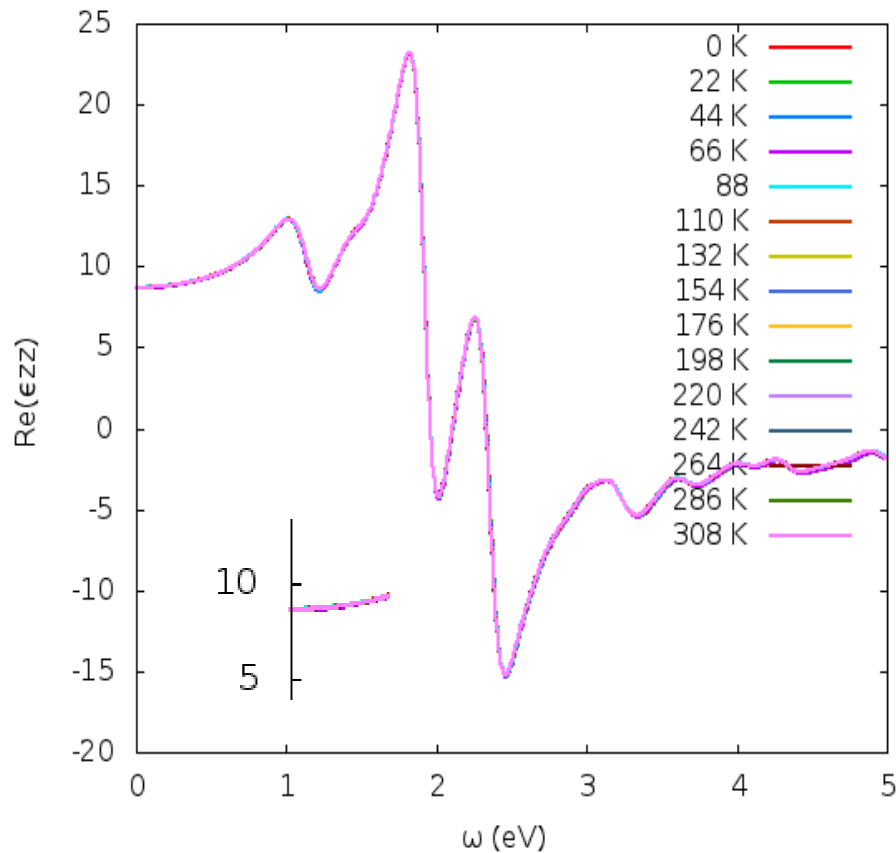


Fig. 7 Graph of Real components of complex dielectric tensor against frequency in [001] direction for temperature range of 0 to 308 K in a step of 22 K., insert shows dielectric tensors at frequency equals to zero (i.e. $\text{Re}[\epsilon_{zz}(\omega = 0)]$)

The dielectric constant (relative permittivity) which is value of the real part of the linear dielectric tensor at frequency equals to zero (i.e. $\text{Re}[\epsilon(\omega = 0)]$) in each of the three directions for temperature range of 0 to 308 K were given in Table 2. The dielectric constants obtained at the [100] and [010] directions for all the temperature have very close values. The highest value of dielectric constants was obtained at 88 K corresponding to lattice constant of 6.053 Å while the lowest value was obtained at 66 K corresponding to lattice constant of 6.052 Å for all the three (3) directions. The values obtained in [001] direction were close to the reported value of 8.2[27]; the highest value obtained is 8.719 while the lowest is 8.655. There is a gap between the dielectric constants obtain within the temperature range of 0 – 66 K with those obtained within the range of 88 – 308 K for the three directions.

Table 3 Temperatures and lattice constants with corresponding dielectric constant (ϵ)(i.e. $\text{Re}[\epsilon(\omega = 0)]$) at each of the directions

Temperature (K)	Lattice Constant (Å)	$\text{Re}[\epsilon(\omega = 0)]$		
		[100]	[010]	[001]
0	6.049	1.387	1.429	8.676
22	6.050	1.386	1.427	8.672
44	6.051	1.383	1.425	8.665
66	6.052	1.379	1.421	8.655
88	6.053	1.437	1.479	8.719
110	6.055	1.434	1.476	8.710
132	6.056	1.431	1.473	8.703
154	6.056	1.429	1.471	8.697
176	6.057	1.428	1.470	8.694
198	6.057	1.428	1.470	8.693
220	6.057	1.428	1.470	8.694
242	6.057	1.428	1.470	8.695
264	6.056	1.429	1.471	8.698
286	6.056	1.431	1.473	8.701
308	6.055	1.432	1.474	8.705

5. Conclusion

In this work; geometry construction and configuration parameters optimization was carried out and the optimal lattice constant was determined for $\text{CH}_3\text{NH}_3\text{SnI}_3$. Geometry relaxation was also performed for the structure. The band structure of $\text{CH}_3\text{NH}_3\text{SnI}_3$ was estimated and the result shows that it has a band gap of 1.051 eV. The lattice constant obtained using phonopy with ZPE is close to experimental reported values with an underestimation of 3.01%. The temperature dependent of lattice constant was studied in the temperature range of 0 to 318 K. At the same temperature range, shift in energy bandgap and dielectric constant due to lattice expansion was also investigated. It was shown that temperature affect the bandgap and dielectric constant of $\text{CH}_3\text{NH}_3\text{SnI}_3$, and subsequently it affect the performance of $\text{CH}_3\text{NH}_3\text{SnI}_3$ perovskite solar cells.

References

- [1] S. F. Völker, S. Collavini and J. L. Delgado, Organic charge carriers for perovskite solar cells *ChemSusChem* **8** (18), 3012-3028 (2015).
- [2] A. Kojima, K. Teshima, Y. Shirai and T. Miyasaka, Organometal halide perovskites as visible-light sensitizers for photovoltaic cells. *Journal of the American Chemical Society* **131** (17), 6050-6051 (2009).
- [3] W. E. Sha, X. Ren, L. Chen and W. C. Choy, The efficiency limit of $\text{CH}_3\text{NH}_3\text{PbI}_3$ perovskite solar cells. *Applied Physics Letters* **106** (22), 221104 (2015).
- [4] T. Oku, Crystal structures of $\text{CH}_3\text{NH}_3\text{PbI}_3$ and related perovskite compounds used for solar cells, in *Solar Cells-New Approaches and Reviews* InTech, (2015).
- [5] A. Abate, Solar Cells Go Lead Free *Joule* (2017).
- [6] S. F. Hoefler, G. Trimmel and T. Rath, Progress on lead-free metal halide perovskites for photovoltaic applications: a review *Monatshefte fur chemie* **148** (5), 795-826 (2017).
- [7] Galadanci GSM and B. Garba, Computations of the Ground State Cohesive Properties Of AlAs Crystalline Structure Using Fhi-Aims Code *IOSR Journal of Applied Physics* **4** (5), 11 (2013).
- [8] P. Hohenberg and W. Kohn, Inhomogeneous Electron Gas *Physical Review* **136** (3B) (1964).
- [9] A. Users' Guide, Fritz Haber Institute ab initio molecular simulations: FHI-aims (2013).
- [10] J. Owolabi, M. Onimisi, S. Abdu and G. Olowomofe, Determination of Band Structure of Gallium-Arsenide and Aluminium-Arsenide Using Density Functional Theory *Computational Chemistry* **4** (03), 73-83 (2016).
- [11] V. E. Henrich and P. A. Cox, The surface science of metal oxides. *Cambridge University Press*, (1996).
- [12] Y. Jiao, F. Zhang and S. Meng, Dye sensitized solar cells Principles and new design, in *Solar Cells-Dye-Sensitized Devices* in *Solar Cells-Dye-Sensitized Devices* InTech, (2011).
- [13] L. Kavan, M. Grätzel, S. E. Gilbert, C. Klemenz and H. J. Scheel, Electrochemical and Photoelectrochemical Investigation of Single-Crystal Anatase *Journal of American Chemical Society* **8** (26), 6716-6723 (1996).
- [14] F. Brivio, A. B. Walker and A. Walsh, Structural and electronic properties of hybrid perovskites for high-efficiency thin-film photovoltaics from first-principles *Apl Materials* **1** (4), 042111 (2013).
- [15] Y. Yuan, R. Xu, H.-T. Xu, F. Hong, F. Xu and L.-J. Wang, Nature of the band gap of halide perovskites ABX_3 (A = $\text{CH}_3\text{NH}_3, \text{Cs}$; B = Sn, Pb; X = Cl, Br, I): First-principles calculations. *Chin. Phys. B* **24** (11), 5 (2015).
- [16] Y. Yamada, T. Nakamura, M. Endo, A. Wakamiya and Y. Kanemitsu, Photoelectronic Responses in Solution-Processed Perovskite $\text{CH}_3\text{NH}_3\text{PbI}_3$ Solar Cells Studied by Photoluminescence and Photoabsorption Spectroscopy *IEEE Journal of Photovoltaics* **5** (1), 401-405 (2015).

- [17]L. Pedesseau, M. Kepenekian, D. Saponi, Y. Huang, A. Rolland, A. Beck, C. Cornet, O. Durand, S. Wang and C. Katan, Dielectric properties of hybrid perovskites and drift-diffusion modeling of perovskite cells. presented at the *Physics, Simulation, and Photonic Engineering of Photovoltaic Devices V*, (unpublished) (2016)
- [18]A. QuantumWise, ReferenceManual/index. html (2017).
- [19]N.-G. Park, Methodologies for high efficiency perovskite solar cells *Nano convergence* **3** (1), 1-13 (2016).
- [20]N. W. Ashcroft and N. D. Mermin, Solid State Physics College ed. *Saunders College Publishing Fort Worth*, (1976).
- [21]C. Christian, Christian, C., Tutorial IV: Phonons, Lattice Expansion, and Band-gap Renormalization Manuscript for Exercise Problems: *Presented at the Hands-on Tutorial Workshop on ab Initio Molecular Simulations at Fritz-Haber-Institut der Max-Planck-Gesellschaft Berlin*. (July, 2015).
- [22]S. Biernacki and M. Scheffler, Negative thermal expansion of diamond and zinc-blende semiconductors Negative thermal expansion of diamond and zinc-blende semiconductors *Physical review letters* **63** (3), 290 (1989).
- [23]V. Blum, R. Gehrke, F. Hanke, P. Havu, V. Havu, X. Ren, K. Reuter and M. Scheffler, Ab initio molecular simulations with numeric atom-centered orbitals *Computer Physics Communications* **180** (11), 2175-2196 (2009).
- [24]W. Setyawan and S. Curtarolo, High-throughput electronic band structure calculations: Challenges and tools. *Computational Materials Science* **49** (2), 299-312 (2010).
- [25]K. Franz and L. Sergey, Tutorial II: Periodic Systems Manuscript for Exercise Problems: *Presented at the Hands-on Tutorial Workshop on ab Initio Molecular Simulations at Fritz-Haber-Institut der Max-Planck-Gesellschaft Berlin*. (August, 2013).
- [26]G. Dolling and R. Cowley, The thermodynamic and optical properties of germanium, silicon, diamond and gallium arsenide *Proceedings of the Physical Society* **88** (2), 463 (1966).
- [27]P. Umari, E. Mosconi and F. De Angelis, Relativistic GW calculations on $\text{CH}_3\text{NH}_3\text{PbI}_3$ and $\text{CH}_3\text{NH}_3\text{SnI}_3$ perovskites for solar cell applications *Scientific reports* **4**, 4467 (2014).